

# Casimir Energy for a Fermion Coupled to the Sine-Gordon Model

S.S. Gousheh<sup>\*</sup>, A. Mohammadi<sup>†</sup> and L. Shahkarami<sup>‡</sup>

Department of Physics, Shahid Beheshti University G.C., Evin, Tehran 19839, Iran

December 11, 2012

## Abstract

We compute the Casimir energy for a fermion chirally coupled to a prescribed pseudoscalar field in the form of the soliton of the sine-Gordon model. The classical equations of this system are not analytically solvable. We obtain the bound energies of the Fermi field using a numerical method called the relaxation method, and its continuum scattering wavefunctions by the use of the Runge-Kutta-Fehlberg of order 6. Then, we obtain a linear combination of the obtained scattering states, which is the simultaneous eigenstate of the Hamiltonian and parity. Using the obtained scattering wavefunctions and the parity eigenstates, we are able to calculate both the scattering phase shifts and the phase shifts of the parity eigenstates. The resulting phase shifts are consistent with both the weak and strong forms of the Levinson theorem. Having these phase shifts we can compute the Casimir energy of the system in two different ways. We can use the scattering phase shifts to obtain the Casimir energy, or equivalently add the Casimir energy for each parity, calculated by the phase shift for the corresponding parity. We plot the total Casimir energy and also the Casimir energy of each parity as a function of the parameters of the pseudoscalar field. In the graphs of the total Casimir energy and the Casimir energy of the positive parity as a function of the scale of variations of the pseudoscalar field,  $\mu$ , there is a maximum occurring when a fermionic bound energy level with positive parity crosses the line of zero energy. Since no energy level with negative energy crosses the line  $E = 0$ , as we increase  $\mu$ , there is no maximum in the graph of the Casimir energy of the negative parity. The limits  $\mu \rightarrow 0$  and  $\mu \rightarrow \infty$  of the Casimir energy are the ones we expect. The graph of the Casimir energy is in general an increasing function of the value of the pseudoscalar field at spatial infinity,  $\theta_0$ . In the graphs of the total Casimir energy and the Casimir energy of each parity as a function of  $\theta_0$  there are mild cusps when a bound state crosses  $E = 0$ . Moreover, considering a system consisting of a valence fermion in the ground state, we find that the most energetically favorable configuration is the one with a soliton of winding number one.

## 1 Introduction

In the original papers in 1948, Casimir [1, 2] calculated the force between two uncharged perfectly conducting plates separated by vacuum and found that despite the lack of an external field, there exists a net force on the metallic plates and they attract each other. The Casimir effect arises from the change in the zero-point energy of the system. This change could happen when different boundary conditions are imposed or non-trivial spatial background fields such as solitons are present.

The Casimir effect often is pointed out as an evidence of the reality of the quantum fluctuations of fields in the vacuum. Since the energy of the vacuum does not seem to be observable in any laboratory experiment, the appeal of the Casimir force as a macroscopic manifestation of the quantum zero-point fluctuations has drawn much attention over the decades that followed its discovery. Although there are a vast amount of works [3, 4, 5] in which theorists refer to the Casimir effect as a good evidence of the reality of the vacuum fluctuations, recently some authors [6] believe that this effect gives no

<sup>\*</sup>Electronic address: ss-gousheh@sbu.ac.ir

<sup>†</sup>Electronic address: a\_mohammadi@sbu.ac.ir

<sup>‡</sup>Electronic address: l\_shahkarami@sbu.ac.ir

support for the subject (reality of the vacuum energy). Their reason is that the Casimir force can be expressed entirely in terms of Feynman diagrams with external legs and without any reference to the vacuum energy.

The Casimir energy and the resulting forces have been investigated for different fields in different geometries, as the boundary conditions of the system, [7]. Also, the majority of the investigations related to this effect concern the calculation of the Casimir forces between the boundaries in arbitrary spatial dimensions. This force could be either repulsive or attractive. The fact that the energy of a fluctuating field diverges both in the free space vacuum and in a vacuum in which a boundary condition or a background field is imposed, have been known for many years [8]. Many different regularization schemes or renormalization programs have been proposed to cancel these divergences when we subtract the energy of the free space vacuum from the energy of the vacuum in the presence of the boundary conditions or the background fields to find the Casimir energy [9].

One of the first experimental attempts to observe this phenomenon was conducted by Sparnaay [10] in 1958. Their measurement with parallel plates, though not in contradiction with the Casimir theory, could not be an evidence for the Casimir effect, due to large experimental errors. Quantitative experimental confirmation was just possible after the advent of the high precision probes in the 1990s. In 1997 Lamoreaux [11, 12] conducted the first successful measurement for the Casimir effect using a plate and a part of a sphere with a large radius rather than two parallel plates which would require accurate alignment to ensure they are parallel. Since then, many experimental investigations have measured the Casimir force in different shapes of the boundary conditions [13].

Recently, there have been many studies to use the Casimir force for practical applications. As device dimensions for Micro and Nano Electromechanical Systems (MEMS and NEMS) decrease, forces such as the Casimir forces which are normally neglected in macro systems have to be considered. The Casimir force could hinder MEMS and NEMS because it could cause the tiny elements in the device to stick together and helps us to design the wear-proof nano-scale systems [14, 15, 16, 17, 18].

As mentioned above, the zero-point energy can also be affected by the presence of non-trivial background fields which are usually chosen to be soliton. Also sometimes a very simple potential such as an electric potential well is chosen as the background field. This simple choice renders the problem of vacuum polarization and the Casimir energy exactly solvable and helps us to see more details [19]. Some authors compute the Casimir energy as the lowest order quantum correction to the mass of the soliton for models containing solitons such as supersymmetric solitons [20, 21, 22, 23, 24, 25]. For most of the models with solitons, the problem is not exactly solvable and the Casimir energy cannot be calculated directly. However, it can be calculated by the use of the indirect methods such as the phase shift method which relates the derivative of the phase shift with respect to the momentum to the spectral deficiency in the continuum states [20, 22, 23, 24, 19].

In the present paper we choose a Lagrangian describing a Fermi field coupled to a prescribed pseudoscalar field as a background field, in  $(1 + 1)$  dimensions. The background field is chosen to be in the form of the soliton of the sine-Gordon model. As is well-known, the solution of the sine-Gordon model is a real soliton which means that it is a solitary wave whose energy density profile is asymptotically in time restored to its original shape and velocity after collision with another soliton. It is important to note that in our model it is not the solution of E-L equation and is just a background field that does not have any dynamics. However, we know that the back-reaction of the fermion on the soliton is small and it changes the shape of the soliton slightly [26, 27]. Thus, it inspired us to investigate this coupled fermion-soliton model with sine-Gordon soliton as a background field. Since the equations of motion of the fermion for our model are not analytically solvable, we solve them using numerical methods and obtain both the bound and the continuum states for the Fermi field. Our purpose is to calculate the Casimir energy for this system and look closely into the details of this energy for our system. To this end we obtain the Casimir energy of the positive and negative parity eigenstates individually and then we explore these results by comparing them with the bound energy levels of the fermion. For the models with parity symmetry and linear equation of motion, it is possible to find parity eigenstates by mixing independent scattering states in a way that respects parity condition. Each bound energy level has specific parity. Therefore, it is worth to try to find parity eigenstates for continuum states to look closely the system in detail. In this paper, we compare our result with a similar model in which the prescribed pseudoscalar field has a simple piece-wise form which behaves

like a soliton in  $(1 + 1)$  dimensions and the simple form of it makes the problem exactly solvable [28]. We computed the Casimir energy of this simple exactly solvable model (SESM) by subtracting directly the vacuum energy of the system in the presence from the absence of the disturbance [25]. However, it is not possible for the present model, since it is not exactly solvable and it needs another indirect method to calculate the Casimir energy. We take advantage of the phase shift method to calculate it. Moreover, the comparison between these two models helps us to investigate how the functional form of the background field and the details of its shape affect the result for each parity and the scattering ones. Meanwhile, we check the consistency of the Levinson theorem for the phase shift of each parity eigenstate and also the scattering states.

In section II we introduce the model. In section III we explain how to find the bound and continuum states and plot some examples of them. In section IV we focus on the calculation of the Casimir energy by the use of phase shift method. Also, we consider the consistency of the resulting phase shifts with the weak and strong forms of the Levinson theorem. We then show the Casimir energy as a function of the parameters of the pseudoscalar field. In section V we consider a system consisting of a valence fermion present in the ground state, to investigate the stability of the system. In all the sections we compare the results with the ones of SESM. Finally, in section VI we conclude with the brief summary.

## 2 The model of a fermion in the presence of the prescribed sine-Gordon

We couple a Fermi field with a prescribed pseudoscalar field, in the form of the soliton of the sine-Gordon system, through the following Lagrangian

$$\mathcal{L} = \bar{\psi} \left( i\gamma^\mu \partial_\mu - M e^{i\phi(x)\gamma^5} \right) \psi, \quad (1)$$

where the external field  $\phi(x)$  is chosen to be  $\phi(x) = (m/\sqrt{\lambda}) \tan^{-1} [\text{Exp}(mx)] - \pi m/\sqrt{\lambda}$ . The parameters  $M$  and  $m$  refer to the masses of the Fermi and pseudoscalar fields, respectively. Our purpose is to compute the Casimir energy of this system using the spectrum of the Fermi field. The Casimir energy in the standard approach is given by computing the change in the zero-point energy of the field due to the presence of the boundary conditions or the background field. This energy for a Fermi field can be written as follows

$$\begin{aligned} E_{\text{Casimir}} &= \int_{-\infty}^{+\infty} dx \int_0^{+\infty} \frac{dp}{2\pi} \sum_{j=\pm} \left( -\sqrt{p^2 + M^2} \right) \nu_p^{j\dagger} \nu_p^j + \int_{-\infty}^{+\infty} dx \sum_i \left( E_{\text{bound}}^{i-} \right) \chi_{2b_i}^\dagger \chi_{2b_i} \\ &\quad - \int_{-\infty}^{+\infty} dx \int_{-\infty}^{+\infty} \frac{dk}{2\pi} \left( -\sqrt{k^2 + M^2} \right) v_k^\dagger v_k \\ &= \sum_i E_{\text{bound}}^{i-} - \int_0^{+\infty} dk \sqrt{k^2 + M^2} (\rho^{\text{sea}}(k) - \rho_0^{\text{sea}}(k)) + \frac{M}{2}. \end{aligned} \quad (2)$$

The first equality is the relation we derived for the Casimir energy of a Fermi field in [25]. The functions  $\nu_p^j(x)$  and  $v_k(x)$  refer to the normalized fermion wavefunctions for the continuum states with negative energy in the presence and absence of the disturbance, respectively. The functions  $\chi_{2b_i}(x)$  are the normalized fermion wavefunctions for the discrete bound states with negative energy and  $E_{\text{bound}}^{i-}$  denote the energies of these negative bound states. The extra  $M/2$  in the last line takes into account the contribution from the half-bound fermionic state at  $E = -M$  in the free case. The factor  $(\rho^{\text{sea}}(k) - \rho_0^{\text{sea}}(k))$  is the difference between the density of the continuum states with the negative energy in the presence and absence of the disturbance.

If for a system we have all the normalized continuum wavefunctions with negative energy in the presence of the disturbance,  $\nu_p^j(x)$ , and energies of all the negative bound states,  $E_{\text{bound}}^{i-}$ , we can in principle obtain the Casimir energy using any of the two equalities in Eq. (2), though the calculations could be very difficult and we might need to calculate the integrals numerically. In a previous paper

[25] we considered a model described by the Lagrangian (1) in which the pseudoscalar field  $\phi(x)$  is prescribed and in the following form

$$\phi(x) = \begin{cases} -\theta_0 & \text{for } x \leq -l, \\ \mu x & \text{for } -l \leq x \leq l, \\ +\theta_0 & \text{for } l \leq x. \end{cases} \quad (3)$$

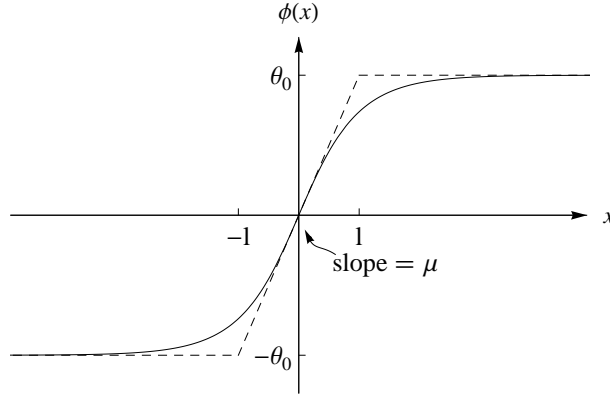


Figure 1: The solid and dashed lines show  $\phi(x)$  for the soliton of sine-Gordon and the simple exactly solvable model, respectively. The parameters  $\theta_0$  and  $\mu$  are also shown in the figure.

This form of  $\phi(x)$  along with the soliton of the sine-Gordon is shown in Fig. (1). In this figure we indicate the parameters  $\theta_0$  and  $\mu$ , which are the value of  $\phi(x)$  at spatial infinities and the slope of the pseudoscalar field at  $x = 0$ , respectively. The form chosen for  $\phi(x)$  in Eq. (3) renders the problem exactly solvable and we are able to obtain the whole spectrum of the fermion as has been done in [28]. Therefore, for this problem we could calculate the Casimir energy by the use of the first equality in Eq. (2). However, in the present problem, the form chosen for the pseudoscalar field makes the equations of motion analytically unsolvable. We can obtain the spectrum of this system by the use of an appropriate numerical method.

It is worth noticing that the expression in the first equality of Eq. (2) only contains the negative energy states. However, in [25] we showed that although the Lagrangian (1) in  $(1+1)$  dimensions is not invariant under the charge conjugation and the particle conjugation symmetries, the total energy density with negative and positive energy are exactly the mirror images of each other for SESM. Therefore, the Casimir energy for this model can be computed only from the negative states or only the positive states, or the average of all of the states and the results are exactly the same in all cases. Note that since all the symmetries of the model with the soliton of the sign-Gordon are the same as SESM, the aforementioned argument is also true for the present model.

### 3 The spectrum of the fermion

The spectrum of a fermion can be totally distorted due to its coupling to a background field. In the presence of the background field the spectral deficiencies can be observed in the continua, and also the bound states can appear. To obtain the distorted fermionic states and their energies in the presence of the prescribed soliton of the sine-Gordon, we start with considering the Dirac equation of the Lagrangian (1). Choosing the representation  $\gamma^0 = \sigma_1$ ,  $\gamma^1 = i\sigma_3$  and  $\gamma^5 = \gamma^0\gamma^1 = \sigma_2$  for the Dirac matrices, this equation becomes

$$i\sigma_1\partial_t\psi - \sigma_3\partial_x\psi - M[\cos\phi(x,t) + i\sigma_2\sin\phi(x,t)]\psi = 0, \quad (4)$$

where  $\psi = \begin{pmatrix} \psi_1 \\ \psi_2 \end{pmatrix}$ . Using the definition  $\xi(x, t) = e^{-iEt} \begin{pmatrix} \xi_1(x) \\ \xi_2(x) \end{pmatrix} = \begin{pmatrix} \psi_1 + i\psi_2 \\ \psi_1 - i\psi_2 \end{pmatrix}$ , the equations obeyed by  $\xi_1(x)$  and  $\xi_2(x)$  can be written in the following matrix form

$$\begin{pmatrix} i\partial_x - E & iMe^{i\phi(x)} \\ -iMe^{-i\phi(x)} & -i\partial_x - E \end{pmatrix} \begin{pmatrix} \xi_1 \\ \xi_2 \end{pmatrix} = \begin{pmatrix} 0 \\ 0 \end{pmatrix}. \quad (5)$$

To obtain the fermionic bound states and their energies, we use a numerical method called the relaxation method, as we did for a similar problem in an earlier paper [27]. This method is used for solving the boundary value problems and it determines the solution by starting with a guess and improving it, iteratively. We refer you to [27] to become familiar with the procedure, in detail. The only difference is that in the present problem here the pseudoscalar  $\phi(x)$  is prescribed and without any dynamics, but  $\phi(x)$  in [27] is not prescribed and is allowed to find its final form through the equations of motion. Therefore, the number of the coupled first-order ODEs in the present problem is less by two. In our problem we use the fermionic bound states and their energies for the exactly solvable model, obtained in [28], as a good initial guess. From now on we rescale all the parameters with respect to the mass of the fermion ( $M$ ), for simplicity.

Figure (2) shows some examples of the bound state energies obtained from the numerical results. The left graph shows the bound energy levels of the fermion as a function of  $\mu$  at  $\theta_0 = \pi$ , i.e. a soliton with winding number one and the right graph shows the bound energies as a function of  $\theta_0$  when  $\mu = 10$ . In both graphs we also depict the bound energy levels of the fermion for SESM, for comparison. The solid and dashed lines refer to the energies of the model with the soliton of sine-Gordon and SESM, respectively. The parity of each bound state is denoted by  $\pm$  signs.

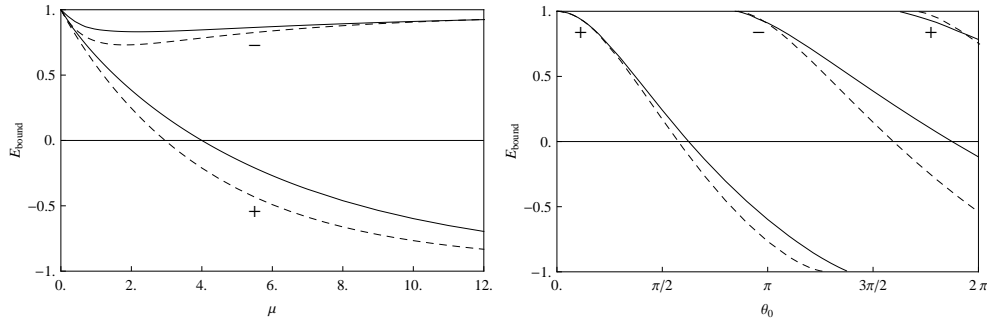


Figure 2: The energies of the bound states of the fermion. The left graph shows the bound energies as a function of  $\mu$  at  $\theta_0 = \pi$  and the right graph shows the bound energies as a function of  $\theta_0$  at  $\mu = 10$ . In both graphs the solid and dashed lines are for the model with the soliton of the sine-Gordon and SESM, respectively. The  $\pm$  signs indicate the parity of each bound state.

Now, we focus on the continuum states. We first obtain the fermion continuum wavefunctions for a scattering process in which a plane wave enters the scattering region from the left. Then, using the scattering wavefunctions, we find the parity eigenfunctions which satisfy the parity condition  $P\xi(x, t) = -\sigma_2\xi(x, t)$ .

Choosing  $\xi_1(x) = \eta_1(x) + i\eta_2(x)$  and  $\xi_2(x) = \eta_3(x) + i\eta_4(x)$  in which in general  $\eta_i$ s are real functions of  $x$ , we obtain the equations of motion satisfied by  $\eta_i$ s in the following form

$$\eta_1' + \cos \phi(x) \eta_3 - E\eta_2 - \sin \phi(x) \eta_4 = 0, \quad (6)$$

$$\eta_2' + \cos \phi(x) \eta_4 + E\eta_1 + \sin \phi(x) \eta_3 = 0, \quad (7)$$

$$\eta_3' + \cos \phi(x) \eta_1 + E\eta_4 + \sin \phi(x) \eta_2 = 0, \quad (8)$$

$$\eta_4' + \cos \phi(x) \eta_2 - E\eta_3 - \sin \phi(x) \eta_1 = 0. \quad (9)$$

For the form chosen for  $\phi(x)$ , i.e. the soliton of the sine-Gordon, we cannot solve this set of equations, analytically. Therefore, we use an appropriate numerical method to find the scattering wavefunctions. We solve this set as an initial value problem and find the wavefunctions for the whole interval  $(-\infty, +\infty)$ , using the so-called Runge-Kutta methods. In order to find the solutions with high accuracy, we use the Runge-Kutta-Fehlberg method of order 6. Since the form chosen for  $\phi(x)$  in SESM is similar to the soliton of the sine-Gordon as  $x \rightarrow \pm\infty$ , we can take advantage of the solutions of SESM to determine the initial boundary values for solving the equations. We already have all the solutions of this model, including the scattering wavefunctions [28, 29]. Figure (3) shows  $\eta_i$ s for the case with the parameters  $\theta_0 = \pi$ ,  $\mu = 10$ ,  $k = 3.0$  and  $E = +\sqrt{k^2 + M^2}$ . This figure also shows  $\eta_i$ s of the SESM, for comparison.

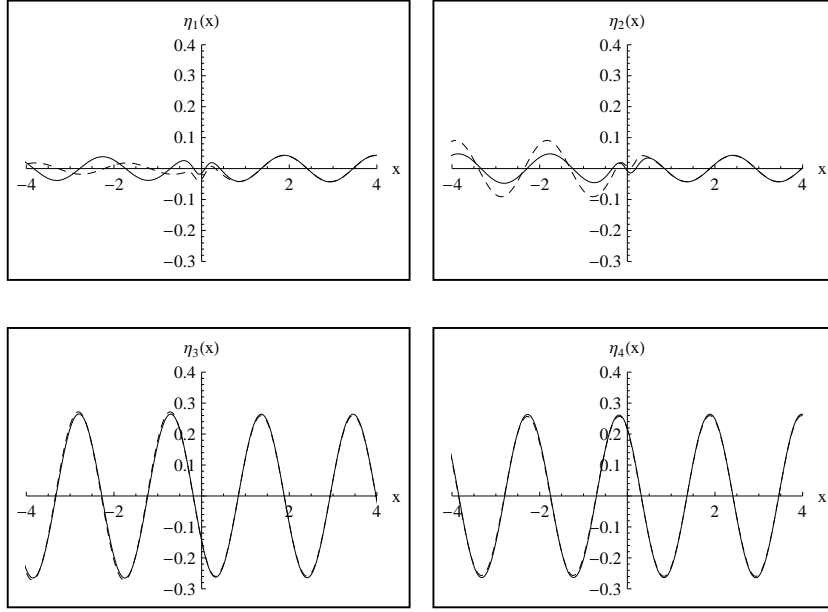


Figure 3: The graphs of  $\eta_i(x)$ s as functions of the spatial variable  $x$ , for the parameters  $\theta_0 = \pi$ ,  $\mu = 10$ ,  $k = 3.0$  and  $E = +\sqrt{k^2 + M^2}$ . The solid and dashed lines show the normalized  $\eta_i(x)$ s for our model and SESM, respectively.

Since the set of equations (5) is a linear set for the Fermi field, a linear combination of its solutions is another solution. We take advantage of this fact to find the continuum parity eigenfunctions. We choose two independent scattering solutions  $\phi_k(x)$  and  $\phi_{-k}(x)$  obtained by the numerical calculations mentioned above. We linearly combine these two solutions and determine the coefficients such that the combined solution becomes the simultaneous eigenstate of the Hamiltonian and the parity operators.

In Figs. (4) and (5) we depict the parity eigenstates for the case with the parameters  $\theta_0 = \pi$ ,  $\mu = 10$ ,  $k = 3.0$  and  $E = +\sqrt{k^2 + M^2}$ . In this figure we also show the continuum parity eigenstates of SESM with dashed lines.  $\begin{pmatrix} y_1^+(x) + iy_2^+(x) \\ y_3^+(x) + iy_4^+(x) \end{pmatrix}$  and  $\begin{pmatrix} y_1^-(x) + iy_2^-(x) \\ y_3^-(x) + iy_4^-(x) \end{pmatrix}$  are the continuum parity eigenstates with the positive and negative parity, respectively. The relations  $y_4^+(-x) = -y_1^+(x)$ ,  $y_2^+(-x) = y_3^+(x)$ ,  $y_4^-(-x) = y_1^-(x)$  and  $y_2^-(-x) = -y_3^-(x)$ , which are equivalent to the parity operation  $P\xi(x, t) = -\sigma_2\xi(x, t)$ , can be easily checked in these graphs.

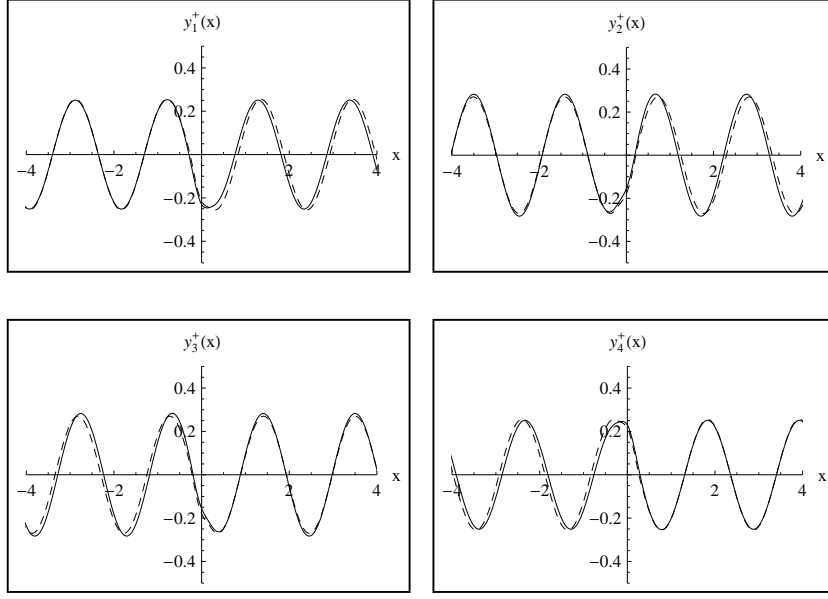


Figure 4: The wavefunction of the fermionic state with positive parity. The graphs of  $y_i^+(x)$ s as functions of the spatial variable  $x$ , for the parameters  $\theta_0 = \pi$ ,  $\mu = 10$ ,  $k = 3.0$  and  $E = +\sqrt{k^2 + M^2}$ . The solid and dashed lines show the normalized  $\eta_i(x)$ s for our model and SESM, respectively.

## 4 The calculation of the Casimir energy using the phase shift method

Now, having all the spectrum of the system, we can calculate the Casimir energy and explore it in detail. The continuum parity eigenstates obtained for our problem are not normalized. Therefore, we cannot directly use the relations given in Eq. (2) to compute the Casimir energy. However, we can utilize the phase shifts of the continuum states to calculate this energy.

### 4.1 The phase shift and Levinson theorem

Our starting point is the following relation

$$\rho(k) - \rho_0(k) = \frac{1}{\pi} \frac{d}{dk} \delta(k), \quad (10)$$

where  $\rho(k) - \rho_0(k)$  is the difference between the density of the continuum states in the free and the interacting cases and  $\delta(k) = \delta^{\text{sky}}(k) + \delta^{\text{sea}}(k)$ , i.e.  $\delta(k)$  sums over the contributions from both positive and negative energies. This relation also holds for the sea and sky, separately.

Substituting Eq. (10) into the second term in the relation of the Casimir energy, Eq. (2), and then integrating by parts, we obtain

$$\begin{aligned} - \int_0^{+\infty} dk \sqrt{k^2 + M^2} (\rho^{\text{sea}}(k) - \rho_0^{\text{sea}}(k)) &= - \int_0^{+\infty} \frac{dk}{\pi} \sqrt{k^2 + M^2} \frac{d}{dk} (\delta^{\text{sea}}(k) - \delta^{\text{sea}}(\infty)) \\ &= \int_0^{+\infty} \frac{dk}{\pi} \frac{k}{\sqrt{k^2 + M^2}} (\delta^{\text{sea}}(k) - \delta^{\text{sea}}(\infty)) + \frac{1}{\pi} M (\delta^{\text{sea}}(0) - \delta^{\text{sea}}(\infty)). \end{aligned} \quad (11)$$

In the first equality we have just subtracted a zero term ( $\frac{d}{dk} \delta^{\text{sea}}(+\infty)$ ) from the original one. Now, we can compute the second term in the expression of the Casimir energy using the phase shift.

Comparing the coefficients of  $e^{ikx}$  on the left- and right-hand sides of the scattering region, we could obtain the scattering matrix element, which is related to the scattering phase shift as  $S(k) = e^{i\delta(k)}$ . As one knows, the parity eigenfunction in both limits  $x \rightarrow \pm\infty$  is a linear combination of  $e^{ikx}$  and  $e^{-ikx}$ .

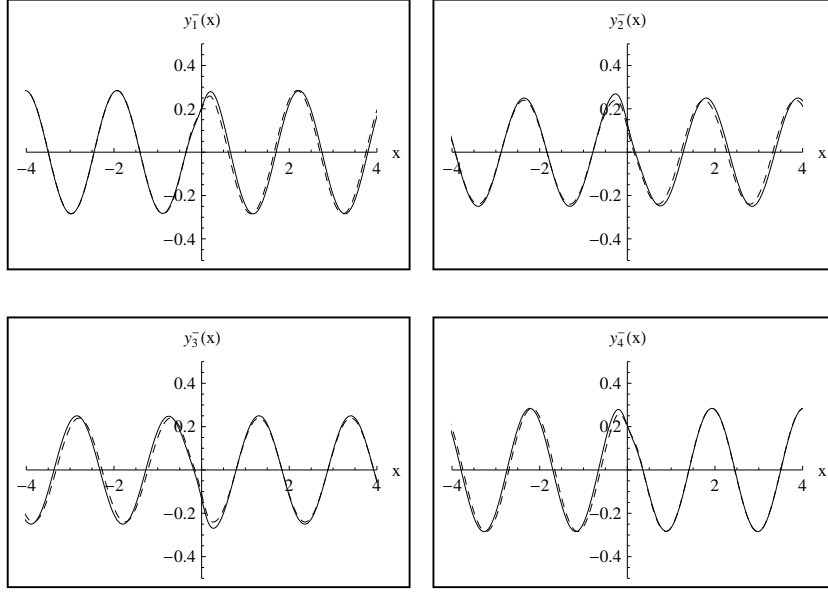


Figure 5: The wavefunction of the fermionic state with negative parity. The graphs of  $y_i^-(x)$ s as functions of the spatial variable  $x$ , for the parameters  $\theta_0 = \pi$ ,  $\mu = 10$ ,  $k = 3.0$  and  $E = +\sqrt{k^2 + M^2}$ . The solid and dashed lines show the normalized  $\eta_i(x)$ s for our model and SESM, respectively.

Thus, the scattering matrix element for parity eigenstates is obtained by comparing the coefficients of  $e^{ikx}$  of the parity eigenfunctions on the left- and right-hand sides and is related to the phase shift as  $S_{\pm}(k) = e^{2i\delta_{\pm}(k)}$ .

Now we check the consistency of the resulting phase shifts with the Levinson theorem. The weak form of this theorem for the Dirac equation is as follows [29]

$$\Delta\delta \equiv [\delta^{\text{sky}}(0) - \delta^{\text{sky}}(\infty)] + [\delta^{\text{sea}}(0) - \delta^{\text{sea}}(\infty)] = \left( N + \frac{N_t}{2} - \frac{N_t^0}{2} \right) \pi, \quad (12)$$

where  $N$  is the total number of bound states, including positive and negative ones,  $N_t$  the total number of the threshold bound states at the given strength of the potential, and  $N_t^0$  the number of bound states at zero strength of the potential, i.e. the free Dirac case. The strong form of the Levinson theorem relates the value of the phase shift at each boundary of the continua to the number of levels which have crossed those boundaries, in the process of building up the disturbance. This form of the theorem can be expressed in the following form for  $k = 0$

$$\delta(0) = (N_{\text{exit}} - N_{\text{enter}}) \pi. \quad (13)$$

This relation holds for each of the continua, separately. For each continuum  $N_{\text{exit}}$  ( $N_{\text{enter}}$ ) is the number of the bound states that exit (enter) that continuum from that boundary ( $E = +1.0$  or  $E = -1.0$ ) as the strength of the potential is increased from zero to its final finite value. In this equation the threshold bound states, mentioned above, should be included in  $N_{\text{exit}}$  and  $N_{\text{enter}}$ , with the coefficient  $1/2$ . Moreover, the strong form of the Levinson theorem for  $k = \infty$  can be written in the following form

$$\delta(\infty) = (N_{\text{enter}} - N_{\text{exit}}) \pi. \quad (14)$$

This relation also holds for each continuum, separately. For each continuum  $N_{\text{exit}}$  ( $N_{\text{enter}}$ ) is the number of the bound states that exit (enter) that continuum from  $k = \infty$  ( $E = +\infty$  or  $E = -\infty$ ) as the strength of the potential is increased from zero to its final finite value. Analogous relations hold between each parity phase shift and the corresponding bound states as follows

$$\Delta\delta_{\pm} \equiv [\delta_{\pm}^{\text{sky}}(0) - \delta_{\pm}^{\text{sky}}(\infty)] + [\delta_{\pm}^{\text{sea}}(0) - \delta_{\pm}^{\text{sea}}(\infty)] = \left( N_{\pm} + \frac{N_{t,\pm}}{2} - \frac{N_{t,\pm}^0}{2} \right) \pi, \quad (15)$$



$$\delta_{\pm}(0) = (N_{\text{exit},\pm} - N_{\text{enter},\pm})\pi \quad \text{and} \quad \delta_{\pm}(\infty) = (N_{\text{enter},\pm} - N_{\text{exit},\pm})\pi. \quad (16)$$

As an example of our results, in Fig. (6) we plot the phase shift for our system as a function of  $k$ , for the parameters  $\theta_0 = \pi$  and  $\mu = 10$ . The left graph shows the  $\delta^{\text{sky}}(k)$ , i.e. the phase shift for the scattering states with the positive energy  $+\sqrt{k^2 + M^2}$  and the right graph shows  $\delta_{\pm}^{\text{sky}}(k)$ , i.e. the phase shift for both parity eigenstates with the positive energy. In both graphs we also depict the phase shift of SESM with the same parameters, for comparison. It is easy to check that the phase shifts depicted in these figures are consistent with both the weak and strong forms of the Levinson theorem. In particular  $\delta^{\text{sky}}(k \rightarrow +\infty) = +\theta_0$  and  $\delta_{\pm}^{\text{sky}}(k \rightarrow +\infty) = +\theta_0/2$ , which are consistent with the results of the adiabatic method of Goldstone and Wilczek [30]. For these parameters we can see from Fig. (2) that two levels (the first one with positive parity and the second one with negative parity) have exited from the sky, and  $N_{t,+}^{0,\text{sky}} = 1$  and  $N_{t,-}^{0,\text{sky}} = 0$  at  $E = +1.0$ . Therefore, using the strong form of the Levinson theorem, we expect  $\delta^{\text{sky}}(0)/\pi = 3/2$ ,  $\delta_+^{\text{sky}}(0)/\pi = 1/2$  and  $\delta_-^{\text{sky}}(0)/\pi = 1$ . Moreover, the equality  $\delta^{\text{sky}}(k) = \delta_+^{\text{sky}}(k) + \delta_-^{\text{sky}}(k)$  holds for every  $k$ .

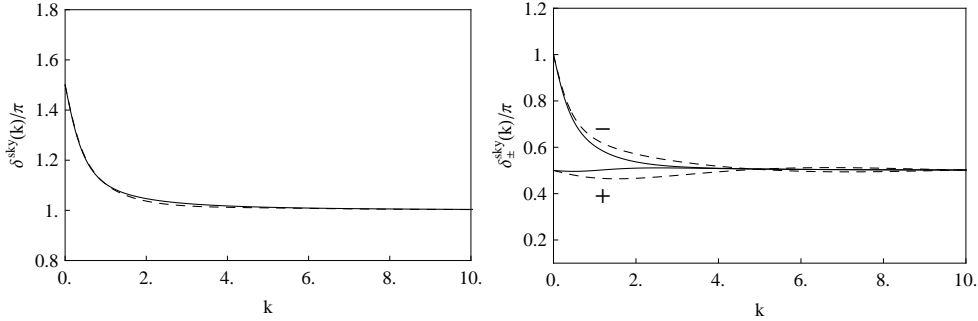


Figure 6: The graphical representation of phase shifts of the continuum states with positive energy, for  $\mu = 10$  and  $\theta_0 = \pi$ . The left graph: the phase shift of the scattering state,  $\delta^{\text{sky}}(k)$ . The right graph: the phase shifts of the  $\pm$  parity eigenstates,  $\delta_{\pm}^{\text{sky}}(k)$ . In both graphs the results for the models with the soliton of sine-Gordon and SESM are shown by the solid and dashed lines, respectively. The  $\pm$  signs in the right graph show the parity of the corresponding eigenstates.

## 4.2 The Casimir energy

Now, using the last expressions in Eqs. (2) and (11) and the bound states shown in Fig. (2) we calculate the Casimir energy for different values of the parameters of the prescribed soliton.

In Fig. (7) we plot the Casimir energy as a function of  $\mu$  at  $\theta_0 = \pi$ , i.e. a soliton with winding number 1, for our model and for SESM by the solid and dashed lines, respectively. The left and right graphs in this figure, respectively, show the total Casimir energy and the Casimir energy for the each parities. The parity of states in the right graph is denoted by the  $\pm$  signs. As can be seen from the left graph, in both models, there is a sharp maximum occurring when the bound energy level crosses the line of  $E = 0$ . This crossing happens for a larger value of  $\mu$  for our model, based on the bound energy levels shown in the left graph of Fig. (2). For our model the bound energy level crosses the line of  $E = 0$  at  $\mu \approx 4.000$ , while for SESM this crossing occurs at the lower value of the slope, i.e.  $\mu \approx 2.957$ . Also, the value of the Casimir energy is lower in the case of the soliton of the sine-Gordon. The largest difference between the graphs of these two models happens around the maximum, as is shown in the zoomed box of the left graph. In both models the Casimir energy reaches the expectable value of zero when the slope of  $\phi(x)$  at  $x = 0$  decreases to zero, i.e. when the vacuum energy approaches that of the trivial vacuum, despite the residual non-trivial boundary conditions. Also, the Casimir energy for both models have the same limit when the slope of the pseudoscalar field tends to infinity. This limit is zero at  $\theta_0 = n\pi$ , i.e. when we have a proper soliton with winding number  $n$ . However, for other values of  $\theta_0$  the Casimir energy is in general non-zero, when  $\mu \rightarrow \infty$  in both models (see Eq. (3.9) in

[25]). From the graphs of the energy for the separated parity states we can see that there is a sharp maximum for the Casimir energy of the positive parity occurring when the first energy level in the left graph of Fig. (2) with positive parity crosses the line of  $E = 0$ . However, the Casimir energy of the negative parity does not have any maximum, since none of the negative parity levels crosses the line of zero energy at  $\theta_0 = \pi$ . The total Casimir energy in the left graph is the sum of the Casimir energy for the positive and negative parity states shown in the right graph. One can indeed calculate the total Casimir energy using the scattering phase shift and the whole bound states of the fermion, or equivalently by adding the Casimir energy obtained for each parity using the phase shift of the parity eigenstates and the corresponding bound states.

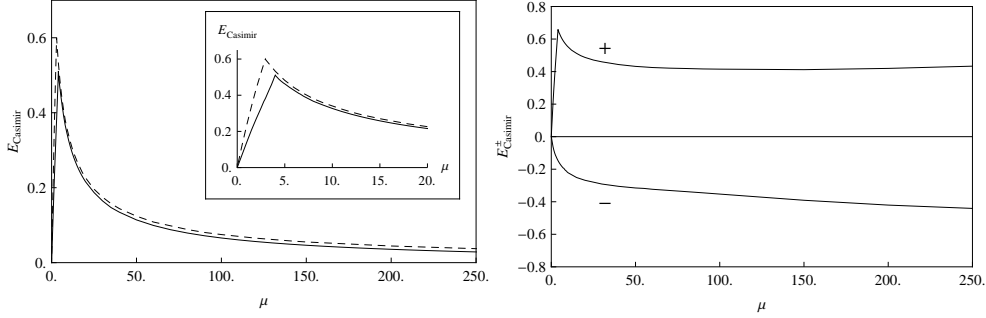


Figure 7: The graphical representation of the Casimir energy as a function of  $\mu$ , the scale of variation of the soliton, at  $\theta_0 = \pi$ . The left graph shows the total Casimir energy for the model with soliton and SESM, with the solid and dashed lines, respectively. In the box we focus on the small values of  $\mu$  to show the details of the maximum and the differences between the results of two models. The right graph shows the Casimir energy for the  $\pm$  parities, separately.

In Fig. (8) we present the Casimir energy as a function of  $\theta_0$  for  $\mu = 10$ , by the solid and dashed lines for the model with the soliton of sine-Gordon and SESM, respectively. As before, the left and right graphs in this figure show the total Casimir energy and the Casimir energy for the each parities, respectively. As can be seen, the total Casimir energy is, on the average, an increasing function of  $\theta_0$  for both models and there are two mild cusps in each graph. Comparing these graphs with the right graph of Fig. (2), we conclude that these cusps occur when the bound energy levels cross the line of  $E = 0$ . The bound energy levels cross  $E = 0$  at  $\theta_0 \approx 0.625\pi$  and  $\theta_0 \approx 1.875\pi$  for our model, and at  $\theta_0 \approx 0.576\pi$  and  $\theta_0 \approx 1.596\pi$  for SESM, in the interval  $0 \leq \theta_0 \leq 2\pi$ . From the right graph it can be seen that the Casimir energy for both parities has a mild cusp occurring where the levels with positive and negative parity cross the line of  $E = 0$ , as expected. As before, the total Casimir energy in the left graph is the sum of the Casimir energy for  $\pm$  parities in the right graph.

## 5 Stability of the solutions

In this section we consider a system consisting of a valence fermion in the ground state and explore the effect of the Casimir energy on its total energy. The total energy for such a system is the sum of the Casimir energy and the energy of the valence fermion. Note that the energy of the valence fermion should not be added when this energy is negative, since it has already been taken into account in the Casimir energy. We show the total energy in Figs. (9) and (10). In the left graph of Fig. (9) we vary the slope  $\mu$  of the prescribed pseudoscalar field while its asymptotic value is fixed at  $\theta_0 = \pi$  and in the right graph of Fig. (10) we plot the total energy for  $\mu = 10$  and different values of  $\theta_0$ . In both graphs the solid and dashed lines refer to the results for the model with the soliton and SESM, respectively. Using the Casimir energy for the individual parities shown in the right graphs, we are able to explore

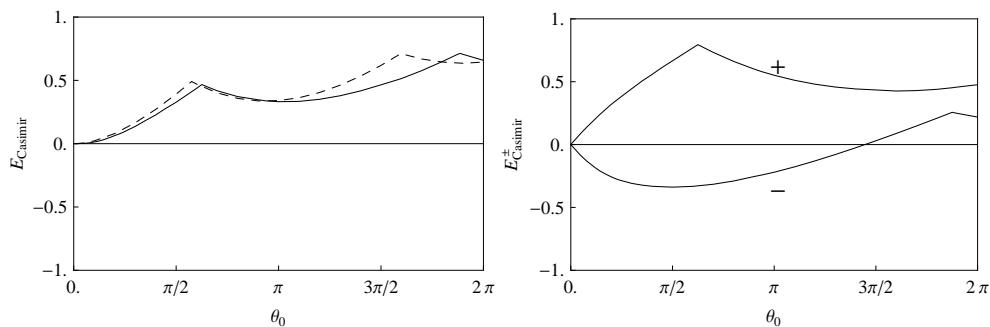


Figure 8: The graphical representation of the Casimir energy as a function of  $\theta_0$ , the value of the soliton at spatial infinity, at  $\mu = 10$ . The left graph shows the total Casimir energy for the model with soliton and SESM, with the solid and dashed lines, respectively. The right graph shows the Casimir energy for the  $\pm$  parities, separately.

the stability of each parity, separately. It should be mentioned that since the ground state of the fermion has positive parity, the total energy for the negative parity has only one contribution coming from the Casimir energy for the negative parity eigenstates. We show the total energy for the positive and negative parities with the  $\pm$  signs. In the right graph we can see an interesting result. For both models there is a minimum occurring at  $\theta_0 \approx \pi$ , which corresponds to a soliton with winding number one. This means that not only this configuration is energetically favorable, but also it is stable against small fluctuations in the parameters of the background field when this field is a soliton with a proper winding number, as expected.

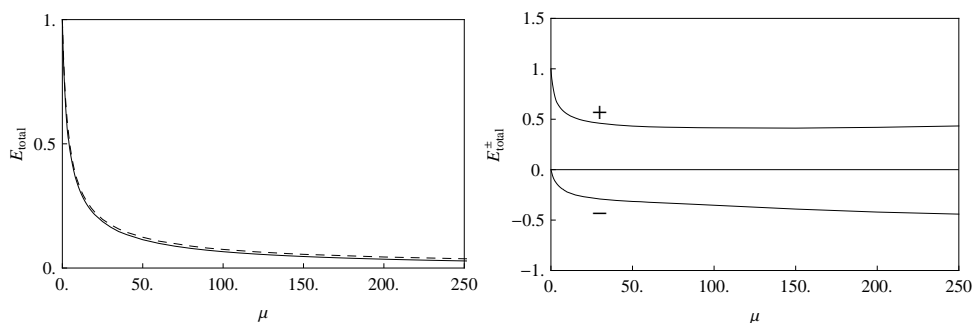


Figure 9: The left graph shows the total energy (the sum of the energy of a valence fermion and the Casimir energy) as a function of  $\mu$  when  $\theta_0 = \pi$ . The solid and dashed lines represent the total energy for the model with the sine-Gordon soliton and SESM, respectively. The right graph shows the total energy for positive and negative parities, separately.

## 6 Conclusion

We compute the Casimir energy for a coupled fermion-pseudoscalar field in which the pseudoscalar field is prescribed and chosen to be the sine-Gordon soliton. This model is not exactly solvable. Therefore, we use the relaxation method and the Runge-kutta-Fehlberg method to obtain the bound states and continuum scattering wavefunctions of the fermion, respectively. Since the model is invariant under the parity and its equations of motion are linear, the parity eigenfunctions of the system can be obtained using a linear combination of the continuum scattering states. The coefficients of this combination

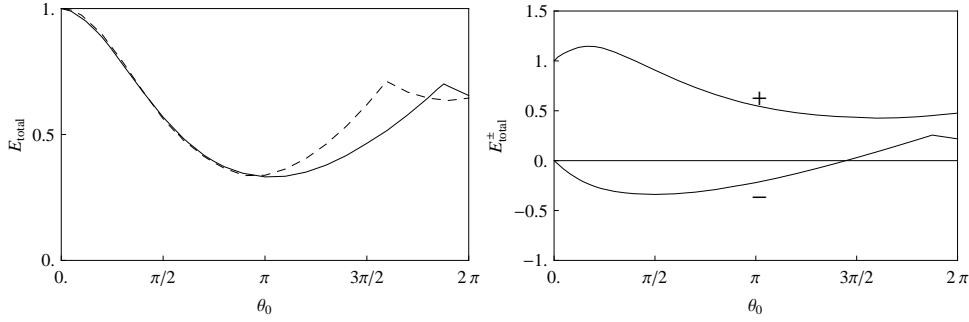


Figure 10: The left graph shows the total energy (the sum of the energy of a valence fermion and the Casimir energy) as a function of  $\theta_0$  when  $\mu = 10$ . The solid and dashed lines represent the total energy for the model with the sine-Gordon soliton and the SESM, respectively. The right graph shows the total energy for positive and negative parities, separately. Notice that the system attains its lowest energy at  $\theta_0 = \pi$ .

are determined by the use of the parity condition. It is interesting to find the continuum parity eigenfunctions, because bound states are eigenstates of the parity. Having all these states, it is possible to investigate the system and all the results for each parity, in detail. To end up with Casimir energy, we use the phase shift method. To be sure about the resulting phase shifts, we check their consistency with the weak and strong Levinson theorems for each parity and scattering phase shifts. Moreover, we compute and plot the Casimir energy as a function of the slope of the pseudoscalar field at  $x = 0$  ( $\mu$ ) and its value at infinity ( $\theta_0$ ). The graph of the Casimir energy as a function of  $\mu$  has a sharp maximum at the value of  $\mu$  in which the fermion has a zero-mode and goes to zero for  $\mu \rightarrow 0$ , and also for  $\mu \rightarrow \infty$  for a soliton with the proper winding number. In the graph of the Casimir energy as a function of  $\theta_0$ , there are some cusps when the fermion bound energies cross the line of  $E = 0$ . Also, we calculate and plot the graph of the Casimir energy as functions of  $\mu$  and  $\theta_0$  for each parity to investigate what exactly happens in the system by comparing them with the fermionic bound energy levels. The Casimir energy obtained by the use of the scattering phase shifts is the sum of the Casimir energy obtained from both parity phase shifts. Finally, we study the stability of the system in the presence of a real fermion in the ground state. We show that the total energy has a minimum, independent of the details of the shape of the background field, for a proper soliton with winding number 1. For each of the graphs we compare the results with SESM that mimics the soliton in  $(1 + 1)$  dimensions.

## Acknowledgement

We would like to thank the research office of the Shahid Beheshti University for financial support.

## References

- [1] H.B.G. Casimir, Proc. Kon. Aa. Wet. **51**, 793 (1948).
- [2] H.B.G. Casimir and D. Polder, Phys. Rev. **73**, 360 (1948).
- [3] S. Weinberg, Rev. Mod. Phys. **61** 1 (1989).
- [4] S.M. Carroll, Living Rev. Relativity **4**, 1 (2001).
- [5] P.J.E. Peebles and B. Ratra, Rev. Mod. Phys. **75**, 559 (2003).
- [6] R.L. Jaffe, Phys. Rev. **D 72**, 021301(R) (2005).
- [7] T.H. Boyer, Phys. Rev. **174**, 1764 (1968); L.L. DeRaad and K.A. Milton, Ann. Phys. (N.Y.) **136**, 229 (1981); X. Li and X. Zhai, J. Phys. A: Math. Gen. **34**, 11053 (2001); D.A.R. Dalvit, F.C. Lombardo, F.D. Mazzitelli and R. Onofrio, Phys. Rev. **A 74**, 020101 (2006); V.B. Bezerra, G.

- Bimonte, G.L. Klimchitskaya, V.M. Mostepanenko and C. Romero, Eur. Phys. J. **C 52**, 701 (2007); R. Moazzemi and S.S. Gousheh, Phys. Lett. **B 658**, 255 (2008); M.A. Valuyan, R. Moazzemi and S.S. Gousheh, J. Phys. B: At. Mol. Opt. Phys. **41**, 145502 (9pp) (2008); S.S. Gousheh, R. Moazzemi and M.A. Valuyan, Phys. Lett. **B 681**, 477 (2009); H. Cheng, Phys. Rev. **D 82**, 045005 (2010); A. Seyedzahedi, R. Saghian and S.S. Gousheh, Phys. Rev. **A 82**, 032517 (2010); N. Graham, A. Shpunt, T. Emig, S.J. Rahi, R.L. Jaffe and M. Kardar, Phys Rev **D 81**, 061701 (2010); E.K. Abalo, K.A. Milton and L. Kaplan, Phys. Rev. **D 82**, 125007 (2010); R. Zandi, T. Emig, U. Mohideen, Phys Rev **B 81**, 195423 (2010); Xiang-Hua Zhai, Xin-Zhou Li and Chao-Jun Feng, Eur. Phys. J. **C 71**, 1654 (2011); L.P. Teo, Phys. Rev. **D 84**, 025022 (2011); L.P. Teo, Phys. Rev. **D 85**, 045027 (2012).
- [8] P. Candelas and D. Deutsch, Phys. Rev. **D 20**, 3063 (1979); P. Candelas and D. Deutsch, Ann. Phys. **143**, 3063 (1982). **check**
- [9] M. Bordag and K. Kiresten, Int. J. Mod. Phys. **A 17**, 813 (2002); S. Ichinose, Int. J. Mod. Phys. **A 23**, 2245 (2008); R. Linares, H.A. Morales-Tecotl and O. Pedraza, Phys. Rev. **D 81**, 126013 (2010); O.G. Kharlanov and V.Ch. Zhukovsky, Phys. Rev. **D 85**, 025015 (2010); Y. Zhu, S. Wu, Y. Liu and Y. Jiang, Phys. Rev. **D 84**, 123002 (2011); M.F. Maghrebi, S.J. Rahi, T. Emig, N. Graham, R.L. Jaffe and M. Kardar, PNAS **108**, 6867 (2011); A.R. Kitson and A.I. Signal, Phys. Rev. **D 85**, 025021 (2012).
- [10] M.J. Sparnaay, Physica **24**, 751 (1958).
- [11] S.K. Lamoreaux, Phys. Rev. Lett. **78**, 5 (1997).
- [12] S.K. Lamoreaux, Phys. Rev. Lett. **81**, 5475(E) (1998).
- [13] A. Roy and U. Mohideen, Phys. Rev. Lett. **82**, 4380 (1999); G. Bressi, G. Carugno, R. Onofrio and G. Ruoso, Phys. Rev. Lett. **88**, 041804 (2002); R.S. Decca, D. López, E. Fischbach, G.L. Klimchitskaya, D.E. Krause and V.M. Mostepanenko, Annals of Physics (N.Y.) **318**, 37 (2005); G. Bimonte, D. Born, E. Calloni, G. Esposito, U. Huebner, E. Il'ichev, L. Rosa, F. Tafuri and R. Vaglio, J. Phys. A: Math. Theor. **41**, 164023 (8pp) (2008); M. Masuda and M. Sasaki, Phys. Rev. Lett. **102**, 171101 (2009); R.S. Decca, Int. J. Mod. Phys. **A 26**, 3910 (2011).
- [14] H.B. Chan, V.A. Aksyuk, R.N. Kleiman, D.J. Bishop and F. Capasso, Science **291**, 1941 (2001).
- [15] H.B. Chan, V.A. Aksyuk, R.N. Kleiman, D.J. Bishop and F. Capasso, Phys. Rev. Lett. **87**, 211801 (2001).
- [16] A. Ashourvan, M.F. Miri and R. Golestanian, Phys. Rev. Lett. **98**, 140801 (2007).
- [17] A. Ashourvan, M.F. Miri and R. Golestanian, Phys. Rev. **E 75**, 040103 (R) (2007).
- [18] M.F. Miri and R. Golestanian, Appl. Phys. Lett. **92**, 113103 (2008).
- [19] Z. Dehghan and S.S. Gousheh, IJMPA **27**, 1250093 (2012).
- [20] R.F. Dashen, B. Hasslacher and A. Neveu, Phys. Rev. **D 10**, 4130 (1974).
- [21] J. Verwaest, Nucl. Phys. **B 123**, 100 (1977); L.D. Faddeev and V.E. Korepin, Phys. Rept. **42**, 1 (1978); S.G. Naculich, Phys. Rev. **D 46**, 5487 (1992); M. Bordag, A.S. Goldhaber, P. van Nieuwenhuizen and D. Vassilevich, Phys. Rev. **D 66**, 125014 (2002); A. Rebhan, P. van Nieuwenhuizen and R. Wimmer, New J. Phys. **4**, 31 (2002); G. Mussardo, V. Riva and G. Sotkov, Nucl. Phys. **B 699**, 545 (2004); A.S. Goldhaber, A. Litvintsev and P. van Nieuwenhuizen, Phys. Rev. **D 67**, 105021 (2003); A. Rebhan, P. van Nieuwenhuizen and R. Wimmer, Nucl. Phys. **B 679**, 382 (2004).
- [22] A. Rebhan and P. van Nieuwenhuizen, Nucl. Phys. **B 508**, 449 (1997).
- [23] E. Farhi, N. Graham, R.L. Jaffe and H. Wiegel, Nucl. Phys. **B 585**, 443 (2000).
- [24] E. Farhi, N. Graham, R.L. Jaffe and H. Wiegel, Phys. Lett. **B 475**, 335 (2000).

- [25] L. Shahkarami, A. Mohammadi and S.S. Gousheh, JHEP **11**, 140 (2011).
- [26] R. Jackiw, Rev. Mod. Phys. **49**, 681 (1977).
- [27] L. Shahkarami and S.S. Gousheh, JHEP **06**, 116 (2011).
- [28] S.S. Gousheh and R. López-Mobilia, Nucl. Phys. **B 428**, 189 (1994).
- [29] S.S. Gousheh, Phys. Rev. **A 65**, 032719 (2002).
- [30] J. Goldstone and F. Wilczek, Phys. Rev. Lett. **47**, 986 (1981).